Supporting Information

for

Lipopolysaccharide Density and Structure Govern the Extent and Distance of Nanoparticle Interaction with Actual and Model Bacterial Outer Membranes

Kurt H. Jacobson[a,1,2], Ian L. Gunsolus[b,1], Thomas R. Kuech[c], Julianne M. Troiano[d], Eric S. Melby[c], Samuel E. Lohse[e,3], Dehong Hu[f], William B. Chrisler[f], Catherine J. Murphy[e], Galya Orr[f], Franz M. Geiger[d], Christy L. Haynes[b,*], Joel A. Pedersen[a,c,g,*]

[a] Department of Civil and Environmental Engineering, University of Wisconsin, Madison, WI, 53706; [b] Department of Chemistry, University of Minnesota, Minneapolis, MN, 55455; [c] Environmental Chemistry and Technology Program, University of Wisconsin, Madison, WI, 53706; [d] Department of Chemistry, Northwestern University, Evanston, IL, 60208; [e] Department of Chemistry, University of Illinois at Urbana-Champaign, Urbana, IL, 61801; [f] Environmental Molecular Sciences Laboratory, Pacific Northwest National Laboratory, Richland, WA, 99352; [g] Department of Chemistry, University of Wisconsin, Madison, WI, 53706

[1] K.H.J and I.L.G. contributed equally to this work; [2] Present address: Department of Environmental Systems Science, ETH Zürich, Zürich, Switzerland; [3] Present address: Department of Chemistry, Colorado Mesa University, Grand Junction, CO, 81501

[*]Corresponding authors: chaynes@umn.edu, joelpedersen@wisc.edu

Contents

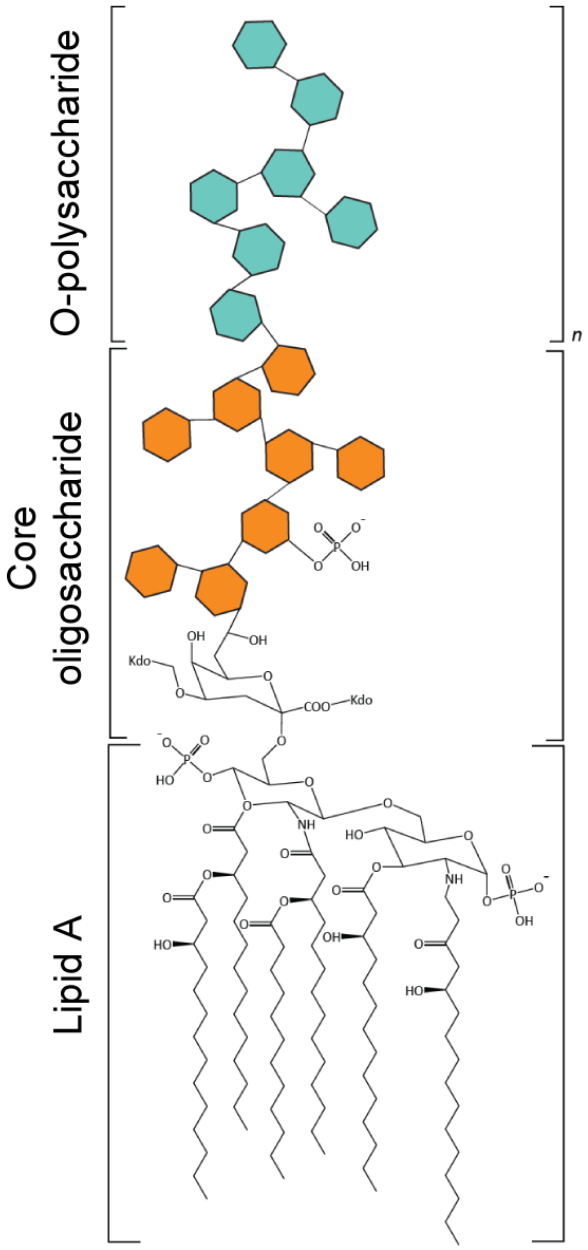

Figure S1. Representation of the general structure of lipopolysaccharide (LPS) from gram-negative bacteria such as *Salmonella enterica*.[1] The LPS molecule can be divided into three domains: Lipid A, the core oligosaccharide, and the O-polysaccharide (or O-antigen). The fatty acid chains of Lipid A vary in number and length depending on the bacterial species and anchor the LPS molecule in the outer leaflet of the outer membrane. These are bound to a phosphorylated glucosamine disaccharide. The core oligosaccharide is covalently bound to Lipid A and contains two or three 2-keto-3-deoxy-D-*manno*-octonate (Kdo) repeat units[2,3] and

commonly L-glycero-D-*manno*-heptose, in addition to other saccharides such as galactose, glucose and glucuronic acid.[4] Some of these saccharides might also be phosphorylated. The outermost domain of LPS is the O-polysaccharide, a repeating oligosaccharide composed primarily of hexoses such as galactose, abequose, mannose, and rhamnose. The presence or absence (or reduction to a non-repeating oligosaccharide)[5] of the O-polysaccharide is used to classify LPS as smooth or rough, respectively. The length and degree of branching of polysaccharide chains varies across bacterial strains and species, but the overall three-component LPS structure depicted is conserved.

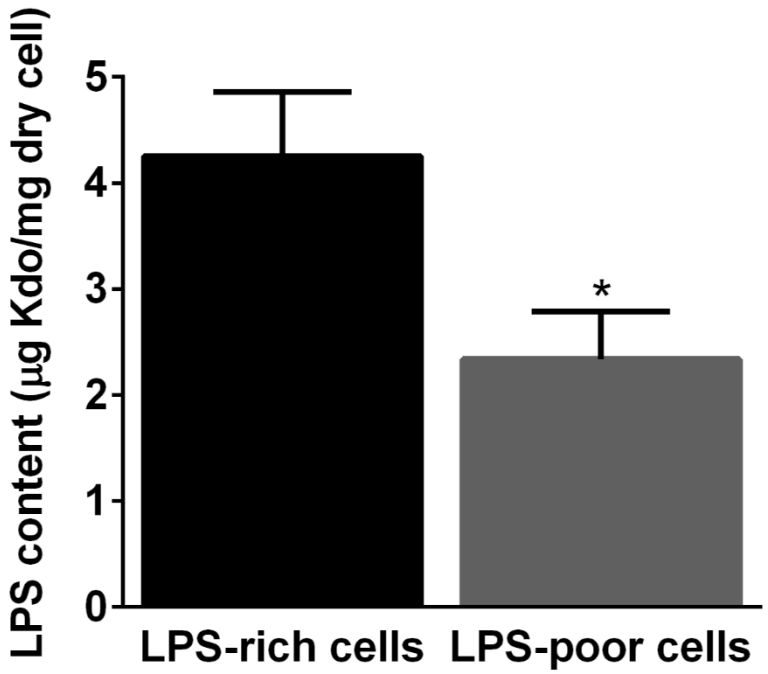

Figure S2. Lipopolysaccharide content of native (no EDTA treatment) and LPS-depleted (EDTA-treated) *Shewanella oneidensis* MR-1 quantified by colorimetric detection 8-amino-3,8-dideoxy-D-*manno*-octulosonic acid (8-amino-Kdo).[6] Error bars represent the standard deviation of three replicate measurements. The 8-amino-Kdo content of LPS-depleted cells is significantly lower than that of native cells ($p < 0.05$), indicated by a single asterisk.

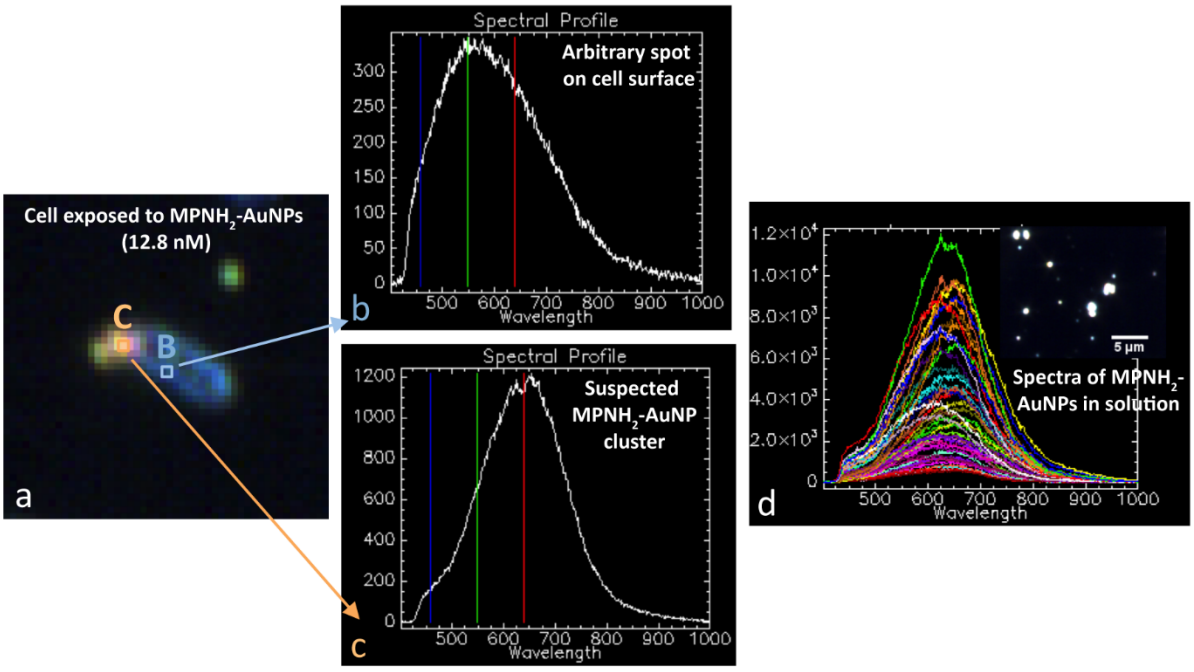

Figure S3. (a) The dark-field micrograph of a single *Shewanella* cell after 10-min exposure to 12.8 nM $MPNH_2$-functionalized gold nanoparticles ($MPNH_2$-AuNPs) (top panel, Figure 3b). A dark-field micrograph was acquired using an Olympus BX43 microscope (Olympus America, Inc., Center Valley, PA) modified with a high signal-to-noise condenser (CytoViva, Auburn, AL). A visible-near infrared (VNIR) spectral map of the cell with approximately 2.8 nm vertical and lateral resolution was acquired using the push-broom technique. An in-line spectrophotometer (Specim, Oulu, Finland) and CCD camera (pco.pixelfly, PCO, Kelheim, Germany) recorded scattered light intensity as the sample stage automatically and incrementally moved the sample into the spectrograph's field of view. Using this technique, a unique VNIR spectrum was acquired for each pixel within the dark-field image. Two pixels are highlighted, and their corresponding spectra are presented in panels **(b)** and **(c)**. Panel B shows the spectrum obtained from an arbitrary spot on the cell surface. This spectrum is representative of the spectra obtained over the entire surface of the cell, excluding the suspected nanoparticle cluster shown in Panel C. At this location (and neighboring locations within the yellow cluster in the dark-field image), the scattered light intensity is approximately four times higher and red-shifted relative to elsewhere on the cell surface. The spectrum obtained from Point C overlaps with spectra acquired from $MPNH_2$-functionalized gold nanoparticles in solution (**d**). Similarity analysis performed using the Spectral Angle Mapping feature of ENVI 4.8 software (Exelis Visual

Information Solutions, Boulder, CO) indicates higher than 90% similarity between spectra obtained from the yellow cluster in the dark-field image and the library of spectra obtained from $MPNH_2$-functionalized gold nanoparticles in solution. This suggests that the yellow cluster associated with the cell surface is composed of $MPNH_2$-functionalized AuNPs.

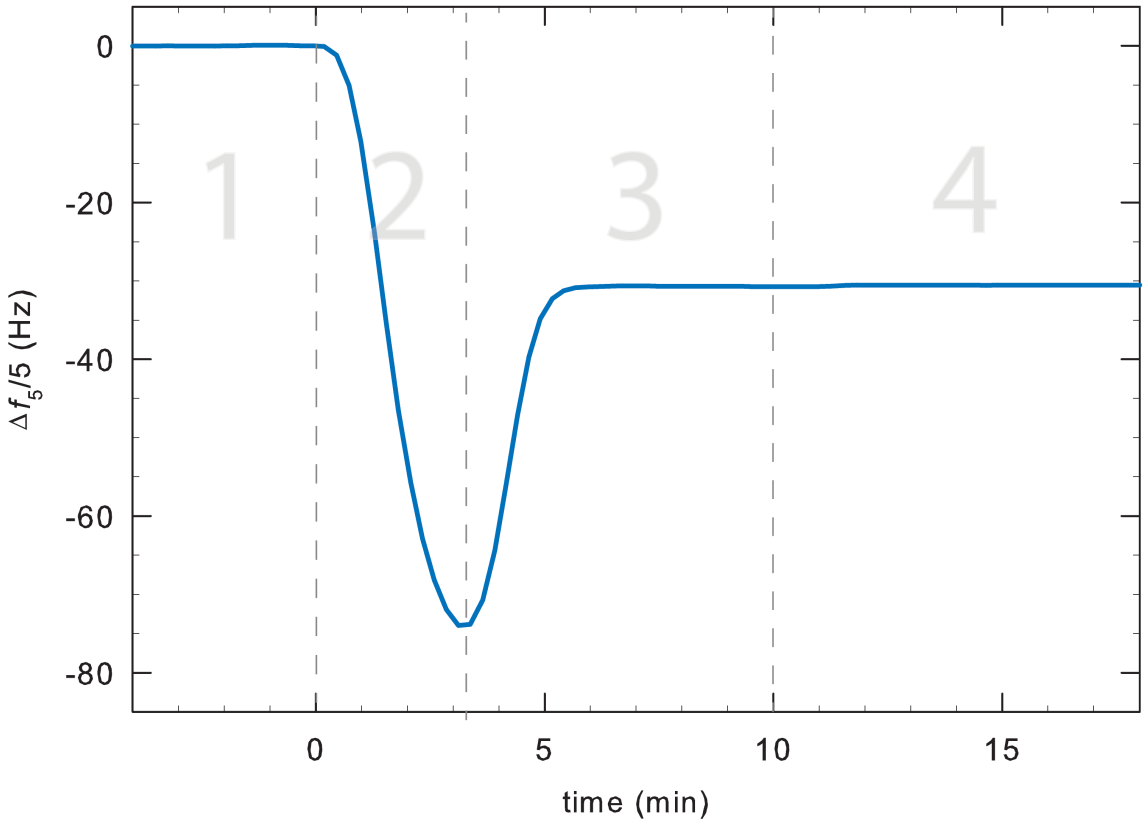

Figure S4. Formation of a representative POPC bilayer containing 0.21 mol % smooth LPS from *Salmonella enterica* serotype minnesota (sLPS) monitored by quartz crystal microbalance with dissipation monitoring (QCM-D). The plot show normalized changes in the frequency of the 5th harmonic ($\Delta f_5/5$). Stable bilayer masses calculated using the Sauerbrey equation[7,8] are presented in Table S1. After the SiO_2-coated QCM-D sensors attained a stable frequency signal under lipid free buffer (Zone 1), a solution containing vesicles (0.125 mg·mL^{-1}) was introduced to the flow cell (Zone 2). Intact vesicles associate with the SiO_2 surface until a critical vesicle coverage is attained and the vesicles rupture and fuse to form a bilayer (Zone 3). The water previously trapped in the vesicles is released, causing a decrease in the measured frequency. Any loosely bound lipid molecules or un-ruptured vesicles are then rinsed away with a lipid free buffer (Zone 4).

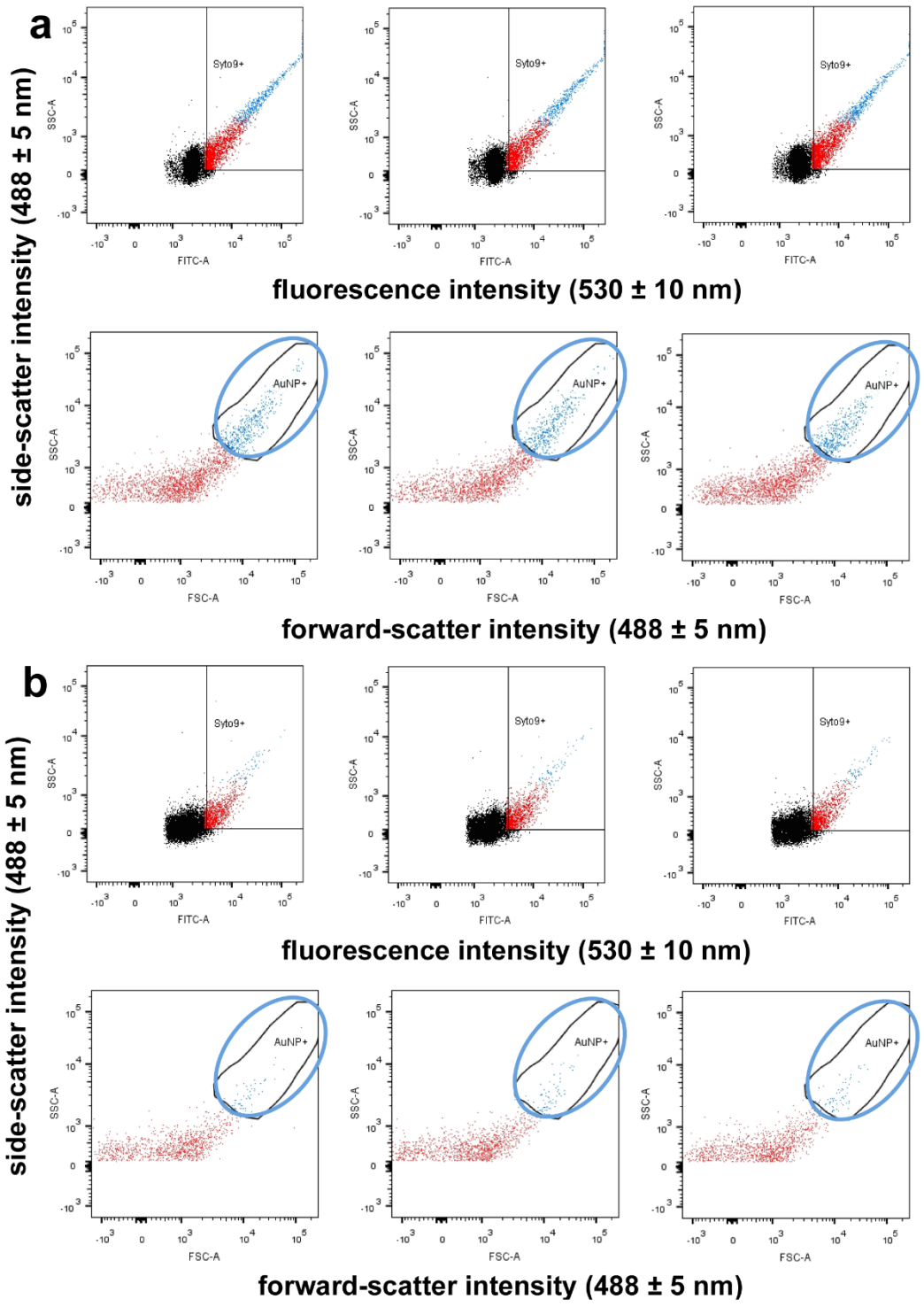

Figure S5. $MPNH_2$-functionalized gold nanoparticles ($MPNH_2$-AuNPs) associate more with native *Shewanella* cells than those depleted in LPS. Triplicate measurements of $MPNH_2$-AuNP association with **(a)** cells with native LPS content (4.25 ± 0.61 μg Kdo/mg dry cell) and **(b)** cells depleted in LPS by brief treatment with EDTA[9] (2.34 ± 0.45 μg Kdo/mg dry cell). The following

abbreviations are used as axes labels: SSC-A (orthogonal or side-scattered light intensity); FITC-A (fluorescence emission intensity in the range 530 ± 10 nm); FSC-A (forward-scattered light intensity). Black points indicate electronic noise and cell debris excluded from analysis; red points indicate cells stained with the nucleic acid stain SYTO-9; blue points indicate cells stained with SYTO-9 with cell-associated gold nanoparticles. In both panels, the top set of bivariate plots display events recorded by the flow cytometer as a function of fluorescence intensity (in the emission window of SYTO-9) and side-scattered light intensity. The boxed region in the top bivariate plots was gated using the minimum SYTO-9 fluorescence intensity of cells stained with SYTO-9, based on controls not exposed to AuNPs. This region, which contains all cells above the threshold staining intensity, acts as the reference population to calculate percent association of gold nanoparticles to cells. The bottom set of bivariate plots display only the events contained within the boxed region of the plots above, plotted using side-scattered vs. forward-scattered light intensity. The region highlighted by a blue circle was gated using the maximum side-scattered light intensity corresponding to cells not exposed to gold nanoparticles. Side-scattered light intensity above this threshold was contributed by the presence of gold nanoparticles, based on controls of gold nanoparticles without cells. The size of this region, corresponding to cells with association gold nanoparticles, decreases significantly with removal of LPS, as seen by comparing the size of this population from the plots in panels **(a)** and **(b)**.

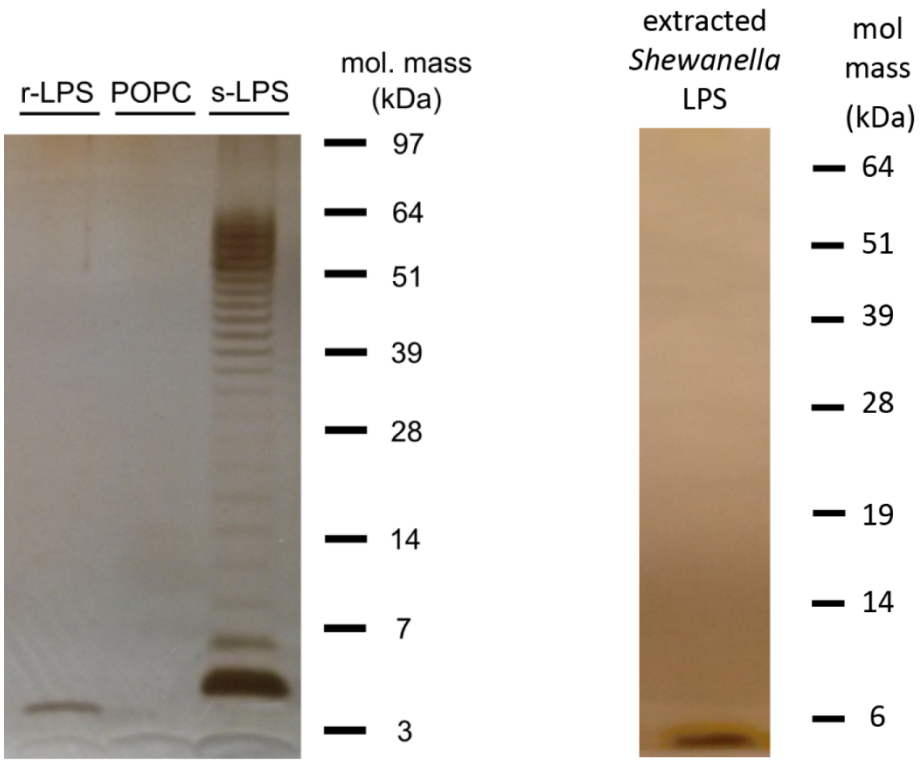

Figure S6. (a) SDS-PAGE/silver staining reveals the much larger average molecular mass of smooth LPS (sLPS, left) than rough LPS (rLPS, right) from *Salmonella enterica* serotype minnesota. POPC shown for comparison (does not stain). **(b)** LPS extracted from *Shewanella oneidensis* MR-1 using the method of Galanos et al.[11] shows similar molecular mass as rough LPS from *Salmonella*.

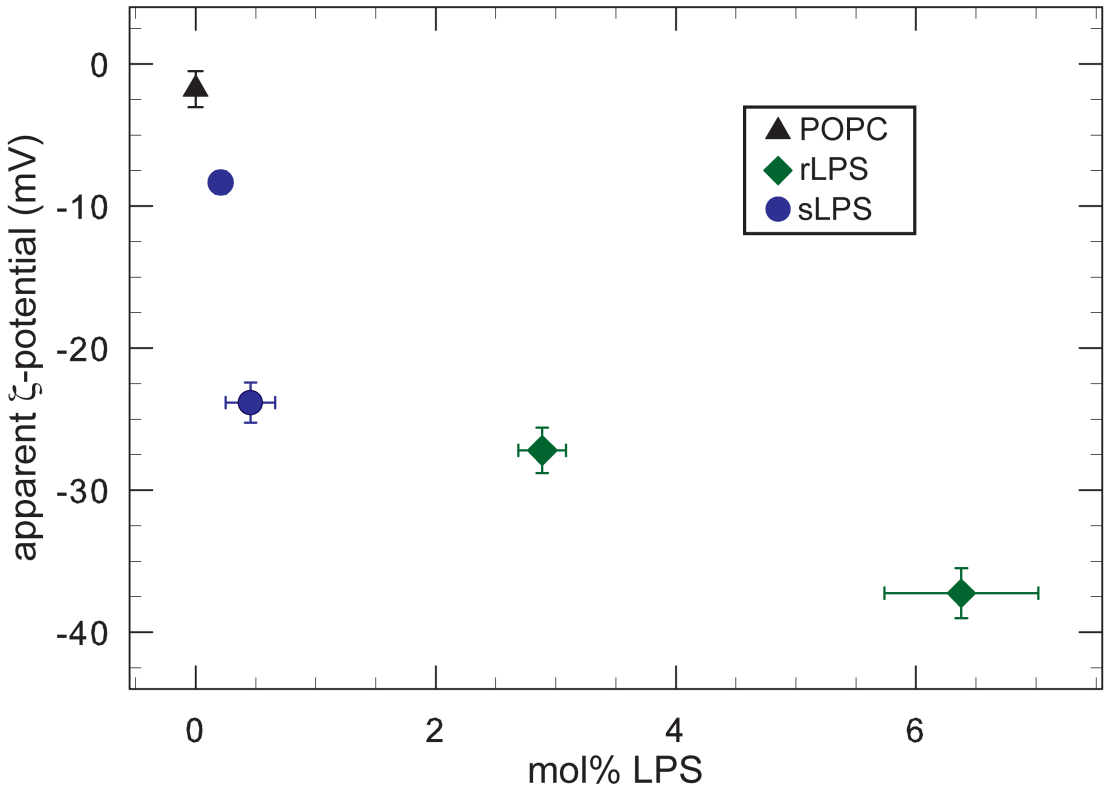

Figure S7. Apparent ζ potentials of unilamellar vesicles composed of POPC or POPC and the indicated mole percent of either smooth LPS (sLPS) or rough LPS (rLPS). Apparent ζ potentials were calculated from the electrophoretic mobility measurements using the Smoluchowski equation.

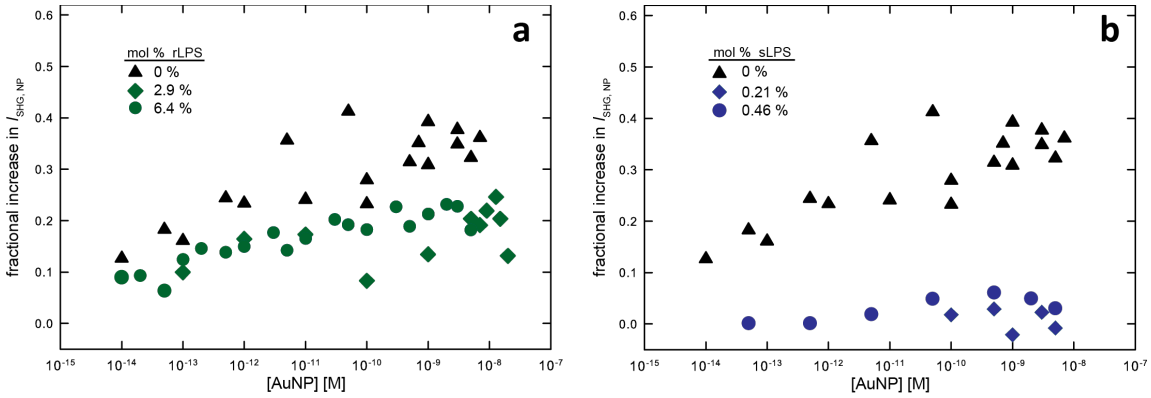

Figure S8. Observed changes in SHG signal intensity following introduction of $MPNH_2$-AuNPs to **(a)** smooth LPS (sLPS)-containing POPC bilayers and **(b)** rough LPS (rLPS)-containing bilayers due to nanoparticle-induced resonance enhancement near the bilayer-solution interface. All experiments were performed in 0.002 M HEPES (pH 7.4) and 0.025 M NaCl. Uncertainties on each SHG *E*-field are < 1% as given by the Poisson statistics of photon counting.

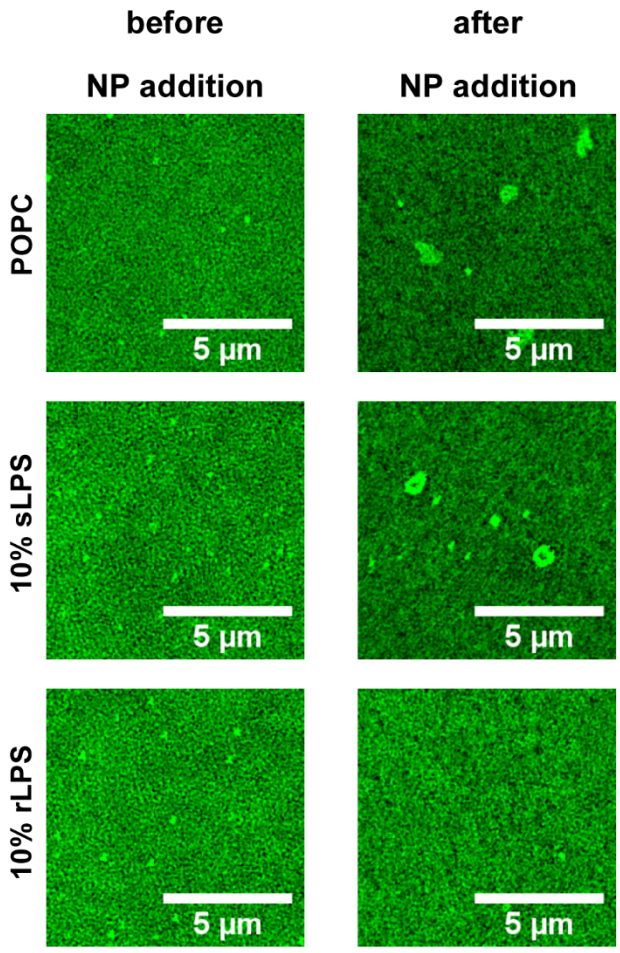

Figure S9. Fluorescence micrographs of LPS-containing POPC bilayers incorporating 0.1 mass percent POPC tagged with the fluorophore dipyrromethene boron difluoride before and after introduction of 12.8 nM (number density) $MPNH_2$-functionalized gold nanoparticles. Changes in lipid ordering following nanoparticle introduction are observed by the formation of bright clusters, regions with enriched fluorescent lipid concentration.

Table S1. Areal acoustic mass densities ($\Delta m_{QCM\text{-}D}$) of SiO_2-supported bilayers composed of POPC and lipopolysaccharide

	mol% LPS		frequency, $\Delta f_5/5$ (Hz)*		dissipation, $\Delta D_5/5$ ($\times 10^6$)*		$\Delta m_{QCM\text{-}D}$ ($ng \cdot cm^{-2}$)†	
bilayer composition	mean	std. dev.	mean	std. dev.	mean	std. dev.	mean	std. dev.
100% POPC	–	–	−25.42	0.26	0.375	0.078	458‡	4.6
9:1 POPC:rLPS	2.9	0.20	−26.15	0.38	0.133	0.016	471§	6.8
8:2 POPC:rLPS	6.4	0.64	−26.36	0.22	0.288	0.136	474§	3.9
9:1 POPC:sLPS	0.21	0.05	−30.05	0.24	1.577	0.030	541¶	4.3
8:2 POPC:sLPS	0.46	0.21	−32.17	0.45	1.920	0.101	579#	8.0

* Means and standard deviations from at least 12 bilayers of each composition

† Calculated using the Sauerbrey equation (5)

‡, §, ¶, # Statistically distinct areal mass densities

Table S2. Final frequency shifts ($\Delta f_5/5$) following AuNP association with LPS-amended POPC bilayers[*]

ionic strength (M)	mol % sLPS	$MPNH_2$-AuNPs $-\Delta f_5/5$ (Hz)	mol % rLPS	$MPNH_2$-AuNPs $-\Delta f_5/5$ (Hz)
0.025	0	11.3 ± 0.4	0	11.3 ± 0.4
	0.21	16.4 ± 1.3	2.9	18.0 ± 0.7
	0.46	19.8 ± 0.9	6.4	25.1 ± 0.6
0.1	0	1.3 ± 0.2	0	1.3 ± 0.2
	0.21	8.5 ± 0.9	2.9	10.3 ± 0.5
	0.46	8.2 ± 1.5	6.4	10.2 ± 0.6

[*] No detectable attachment of MPA-AuNPs.

TABLE S3. Estimated final acoustic areal mass densities ($\Delta m_{QCM\text{-}D}$) following AuNP association with LPS-amended POPC bilayers[*]

ionic strength (M)	mol % sLPS	$MPNH_2$-AuNPs $\Delta m_{QCM\text{-}D}$ ($ng \cdot cm^{-2}$)	mol % rLPS	$MPNH_2$-AuNPs $\Delta m_{QCM\text{-}D}$ ($ng \cdot cm^{-2}$)
0.025	0	200 ± 10[†]	0	200 ± 10[†]
	0.21	280 ± 20[‡]	2.9	320 ± 10[†]
	0.46	330 ± 20[‡]	6.4	450 ± 10[†]
0.1	0	23 ± 4[†]	0	23 ± 4[†]
	0.21	170 ± 20[‡]	2.9	190 ± 10[†]
	0.46	140 ± 30[‡]	6.4	190 ± 10[†]

[*] No detectable attachment of MPA-AuNPs.

[†] Acoustic areal mass densities calculated using the Sauerbrey equation.

[‡] Acoustic areal mass densities calculated using Kelvin-Voight continuum viscoelastic modeling.

Chemicals. We purchased 3-mercaptopropionic acid and 3-mercaptopropyl amine from Sigma-Aldrich (St. Louis, MO). EDTA was procured from Ambion Life Technologies. Chloroform solutions of 1-palmitoyl-2-oleoyl-*sn*-glycero-3-phosphocholine (POPC) and TopFluor®-labeled phosphatidylcholine (1-palmitoyl-2-(dipyrrometheneboron difluoride) undecanoyl-*sn*-glycero-3-phosphocholine) were purchased from Avanti Polar Lipids (Alabaster AL). Lipopolysaccharide (LPS) purified from *Salmonella enterica* serotype minnesota (smooth type) and *Salmonella enterica* serotype minnesota Re595 mutant (rough type) were purchased from Sigma-Aldrich (St. Loius, MO). The Re595 LPS is of the deep rough type and is composed of Lipid A and two Kdo residues.[10] Smooth LPS from *Salmonella enterica* labeled with the fluorphore Alexa488 was purchased from Life Technologies (Carlsbad, CA). LPS from *Shewanella oneidensis* MR-1 (cultured as described in the main text) was extracted using the method of Galanos and co-authors[11] and then treated with Benzonase nuclease (Merck, Darmstadt, Germany) to remove co-purified nucleic acids. Smooth LPS (from *Salmonella*) was dissolved in 8:2 (v/v) ultrapure H_2O:methanol, while rough LPS (from both *Salmonella* and *Shewanella*) was dissolved in neat $CHCl_3$. The distribution of molecular masses of each type of LPS was assessed by silver-staining LPS samples that had been separated by sodium dodecyl sulfate-polyacrylamide gel electrophoresis (SDS-PAGE; see Figure S3).

All aqueous solutions were buffered to pH 7.4 (± 0.05) with 0.002 M 4-(2-hydroxyethyl)-1-piperazineethanesulfonic acid (HEPES; Fisher Scientific). The ionic strength (I) was set to the desired level through addition of NaCl. Prior to use, all solutions were passed through a 0.22 μm syringe filter (Millipore, Billerica, MA).

Bacterial culture media. *Shewanella oneidensis* MR-1 was cultured in LB broth purchased from Becton, Dickinson and Company (Franklin Lakes, NJ), and cell EDTA treatment was performed in Dulbecco's phosphate-buffered saline (D-PBS) purchased from Mediatech, Inc. (Manassa, VA).

Cell Sorting by Flow Cytometry. Cells with and without associated AuNPs were sorted on a FACSAria IIU cell sorter equipped with a 488 nm 50 mW laser into 1.5 mL polypropylene

microcentrifuge tubes using a 100 μm nozzle at 138 kPa. Gating for cell sorting was performed as follows: following staining with SYTO 9 to discriminate bacterial cells from other particles of similar sizes (i.e., cell debris), cells were analyzed via forward- vs. side-scattering light collected with a 488/10 bandpass filter. Gold nanoparticles formed a distinctive pattern on orthogonal scatter (Figure S5). Cell populations with and without associated AuNPs were distinguished using as controls SYTO 9-stained cells not exposed to AuNPs (to determine the SYTO 9 fluorescence intensity threshold positively identifying stained cells) and unstained cells exposed to AuNPs (to determine the orthogonal light scattering intensity threshold identifying cells with associated AuNPs).

Preparation of Lipid Vesicles. Lipid vesicles were prepared by mixing solutions of POPC with and without lipopolysaccharides in the desired mass ratios (viz. 100% POPC and 9:1, 8:2 and 7:3 POPC:LPS mass ratios) in glass vials, evaporating off the majority of the solvent under flowing N_2 gas, before evaporating any remaining solvent in a vacuum chamber for 12 h. The lipid/lipopolysaccharide formulations were then hydrated and suspended in a buffered solution (0.002 M HEPES, pH 7.4, I = 0.150 M) and subjected to four cycles of sonication (5 min, Branson 2510 sonic bath, Branson Ultrasonics, Danbury, CT) and flash freezing in liquid N_2. Unilamellar vesicles were then formed by extruding the lipid suspension through a 50 nm polycarbonate membrane filter (Whatman) 15 times using an Avanti 610000 extruder kit. The electrophoretic mobility and number-average hydrodynamic diameter of the extruded vesicles in buffered solutions (0.002 M HEPES, pH 7.4, I = 0.001 M) at 25.0 ± 0.1 °C were determined from laser Doppler micro-electrophoresis and dynamic light scattering (DLS) measurements using a Malvern ZetaSizer Nano ZS (Worcestershire, UK). The mean values and standard deviations reported represent the average of five measurements performed on each of five solutions (25 total measurements). These data are reported in Figure 3 in the main text.

Lipopolysaccharide incorporation was quantified on an absolute basis using the method described by Karkhanis et al.[6] This method selectively converts 3-deoxy-D-*manno*-oct-2-ulosonic acid (also denoted 2-keto-3-deoxy-D-manno-octonate, Kdo), an acidic residue present in all LPS molecules, to a chromophore that can be used to quantify total LPS content. Briefly, a calibration curve was created using

0-10 μg of synthetic Kdo (Sigma Aldrich, St. Louis, MO) dissolved in 0.2 N sulfuric acid. Solutions of LPS-containing lipid vesicles (2.5 $mg \cdot mL^{-1}$) were also dissolved in 0.2 N sulfuric acid. Then all solutions were treated as described above and loaded into acrylic cuvettes.[6] Light absorption at 552 nm from the resultant chromophore was recorded using an OceanOptics USB2000 spectrometer coupled to a MicroPack DH-2000 UV-vis-NIR light source.

Vesicles containing between 0 and 6.4 mol % smooth or rough LPS had hydrodynamic diameters within experimental error (Figure 3a; determined by DLS in 0.002 M HEPES, pH 7.4, I = 0.001 M), consistent with a prior report.[12] Incorporation of increasing amounts of either rough or smooth LPS molecules into the vesicles shifted their electrophoretic mobilities (determined by laser Doppler microelectrophoresis) to more negative values (Figure 3b) as expected given the net negative charge of these molecules. Average electrophoretic mobility (μ_e) declined from small values typical of neutral bilayers (-0.12×10^8 $m^2 \cdot V^{-1} \cdot s^{-1}$) for pure POPC vesicles to more strongly negative values (near -3.0×10^8 $m^2 \cdot V^{-1} \cdot s^{-1}$) for vesicles incorporating 6.4 mol % rough LPS (Figure 3b). Values for μ_e of vesicles formed with rough LPS were more negative than those formed with equal mass percent of smooth LPS. This result is attributable to the higher molecular mass of smooth than rough LPS molecules (Figure S6) leading to the presence of a lower number of smooth than rough LPS molecules for a given mass of LPS incorporated. We determined the amount of LPS in vesicles from their Kdo content [6]. For an equivalent mass of LPS incorporated into vesicles, the number of rough LPS molecules was approximately five times higher than smooth LPS molecules (M_r = 20 to 70 kDa, see Figure 3c).

Quartz Crystal Microbalance with Dissipation (QCM-D) Monitoring. Quartz crystal microbalance with dissipation monitoring measurements were conducted on a Q-Sense E4 instrument (Biolin Scientific, Göteborg, Sweden) containing four sensors mounted in liquid flow cells (QFM 401) that achieve laminar flow across the sensor surface. The temperature was controlled to 25.0 ± 0.5 °C. In QCM-D measurements, changes in the measured resonance frequency (Δf) of an AT-cut piezoelectric quartz crystal can be attributed to changes of mass ($\Delta m_{QCM\text{-}D}$) coupling to the coated surface of the sensor.[13] All experiments reported here used SiO_2-coated sensors (QSX303, Biolin Scientific). To assess

the viscoelastic properties of the adlayer on the sensor surface, the driving voltage to the crystal is switched off at a frequency of ~5 s^{-1}, and the energy dissipation (ΔD) is calculated from the decay in amplitude of the resonator [13]. Here, normalized Δf and ΔD values are reported for the 5th harmonic (~25 MHz.).

All QCM-D experiments were conducted under constant flow conditions (100 μL·min^{-1}) using a peristaltic pump (Isamatec IPC, IDEX, Oak Harbor, Washington). Under these conditions, the sensitivity limit was determined to be ~5 ng·cm^{-2}. POPC or POPC/LPS bilayers were formed on QCM-D sensors *in situ* by flowing a vesicle-containing solution (0.125 mg·mL^{-1} vesicles in 0.002 M HEPES, pH 7.4, I = 0.150 M) over a SiO_2-coated sensor. The association and rupturing of the vesicles to form a lipid bilayer was monitored by QCM-D. Following rinsing with vesicle-free solution of otherwise identical composition, solution ionic strength was adjusted to that desired for nanoparticle attachment experiments (I = 0.025, 0.050 or 0.100 M), and the QCM-D signal was allowed to stabilize ($df_5 \cdot dt^{-1}$ < 0.05 Hz·min^{-1}).[14] Gold nanoparticles (12.8 nM number concentration) suspended in buffer were then pumped through the flow cells until both the Δf and ΔD signals stabilized. Nanoparticle-free buffer was then pumped through the flow cells to measure the detachment of nanoparticles from the POPC or POPC/LPS bilayers.

Estimation of Masses Measured by QCM-D. The frequency shifts recorded by the QCM-D were used to estimate to areal acoustic mass densities in one of two ways depending on the energy dissipation of the adlayer. In both cases, the estimated mass includes the mass of the analyte and any hydrodynamically coupled water. For more rigid adlayers, defined as having a ΔD-to-Δf ratio < 0.4 × 10^{-6},[8] the Sauerbrey equation[7] was used to directly convert measured Δf to adlayer areal mass density ($\Delta m_{\text{QCM-D}}$):

$$\Delta m_{\text{QCM-D}} = -C\frac{\Delta f_n}{n} \tag{S1}$$

where C is the mass sensitivity constant (for the sensor crystals used here, 18 ng·cm^{-2}·Hz^{-1}) and Δf_n is the chance in frequency of the n^{th} harmonic.

For adlayers that were less rigid, Kelvin-Voight continuum viscoelastic modeling of the collected Δf and ΔD data was performed using the QTools software package (version 3.1.25.604).[8,15]

Preparation of Solid-supported LPS-containing Lipid Bilayers. We formed solid-supported LPS-containing bilayers on SiO_2-coated QCM-D sensors via fusion of LPS-containing POPC vesicles.[12] Figure S4 shows a representative trace of the normalized frequency of the fifth harmonic ($\Delta f_5/5$) vs. time measured during the formation of a smooth LPS containing lipid bilayer on a SiO_2 surface. Lipid-free buffer is pumped over the SiO_2 surface until a stable frequency baseline is obtained (Zone 1). Upon introduction of vesicle-containing solutions (Zone 2), $\Delta f_5/5$ decreases as intact vesicles attach to the SiO_2 surface (decreases in frequency correspond to increases in mass associated with the sensor).[16] Vesicle attachment continues until the critical vesicle coverage is attained (maximum change in frequency), at which point the vesicles begin to rupture on the surface and fuse, releasing the water trapped inside them and causing the frequency to increase (Zone 3).[16] After vesicle rupture and fusion, a stable frequency is reached corresponding to the formation of a bilayer on the sensor surface.[16,17] Any poorly bound lipids or vesicles are rinsed away with lipid-free buffer (Zone 4). Bilayer formation kinetics decreased as the amount of LPS in the vesicles increased. The slower rate of bilayer formation was likely due to stronger electrostatic repulsion between the negatively charged SiO_2 sensor surface (point of zero charge = 3.5)[17] and the net negatively charged LPS-containing vesicles. The steady-state frequency shift of the POPC bilayer was consistent with expectations for a well-formed bilayer[16] and corresponded to 60 $Å^2$ per headgroup. Steady-state frequency shifts of rough and smooth LPS-containing bilayers were larger than those composed of pure POPC, indicating retention of LPS in the bilayers. The magnitude of these shifts were larger for smooth LPS- than rough LPS-containing bilayers, likely attributable to the larger mass contribution from the long polysaccharide chains of smooth LPS than the short polysaccharide chains of rough LPS. Furthermore, the smooth LPS was likely more hydrated than the rough LPS.

Stable bilayers were formed containing up to 20% by mass (0.46 mol %) of smooth LPS without the use of divalent cations, in contrast to the one previous report of LPS-containing lipid bilayer formation on SiO_2 by Kaufmann et al.[12] We attribute this difference to origins of the LPS molecules use

in this and the previous study (different species of *Salmonella* with different O-polysaccharide structures). Attempts to form bilayers from vesicles containing 30 mass % smooth LPS proved unsuccessful.

Second Harmonic Generation. As described previously,[18–21] second harmonic generation (SHG) experiments were performed using a regeneratively amplified Ti:Sapphire laser system (Hurricane, Spectra-Physics, 1 kHz repetition rate, 120 fs pulses) pumping an optical parametric amplifier (OPA-CF, Spectra-Physics) tuned to a fundamental wavelength between 610 and 615 nm. Using a variable density filter, the beam was attenuated to 0.4 μJ/pulse for all experiments, which is below the sample damage threshold. The *p*-polarized beam was focused onto the silica/buffer interface at which the bilayer was formed. The beam exiting the sample was passed through a UV-grade Schott filter to remove any radiation other than the signal. The SHG signal was directed into a monochromator set to the SHG wavelength and then into a photomultiplier tube, where it was amplified and collected using a gated single-photon detection system. The SHG signal was detected following our published procedures.[18–21]

All SHG experiments were performed under static conditions. A fused silica hemisphere was placed on top of a custom-built Teflon flow cell and held leak-tight using a Viton O-ring and a clamp. First, HEPES buffer solution (0.002 M, pH 7.4) adjusted to an ionic strength of 0.150 M was introduced into the cell and the SHG response was recorded until a steady signal was attained for at least 15 min. Next, vesicles containing varying amounts of LPS were introduced into the cell and allowed to self-assemble into an LPS-containing lipid bilayer on the silica substrate for 30 min. The bilayer was rinsed with the formation buffer, a steady SHG signal was collected, and then buffer adjusted to an ionic strength of 0.025 M was introduced and used for the remainder of the experiment. Various concentrations of gold nanoparticles (between 10^{-14} and 10^{-8} M number concentration) in buffer were then introduced into the cell, and the SHG signal was monitored until it stabilized for at least 15 min. After five to six nanoparticle solutions were exposed to the bilayer, nanoparticle-free buffer was introduced to the cell to assess the reversibility of the interaction of the particles with the bilayer.

Super-resolution Fluorescence Microscopy. Solid-supported lipid bilayers were formed within 35/22 mm #1.5 glass bottom dishes (PELCO,Willco Wells). Dishes were rinsed with ultrapure water (18

MΩ·cm; MilliQ Advantage A10, Millipore), dried with N_2, and cleaned in a UV/Ozone chamber (PSD Pro Series, Novascan) for 20 min. Cleaned dishes were equilibrated with 0.002 M HEPES, pH 7.4, I = 0.150 M solution for at least 1 h. Vesicles with 0.1 mass% TopFluor PC (Avanti Polar Lipids) were introduced to the dish in the same buffered solution used to equilibrate the dishes (0.0625 mg mL^{-1} vesicle concentration), and bilayer formation was monitored by structured illumination microscopy (ALYRA, Zeiss), using a 63× magnification objective lens. Determining bilayer formation by fluorescence was possible utilizing fluorescence recovery after photobleaching (FRAP) experiments, as non-ruptured vesicles do not recover after photobleaching, whereas solid-supported lipid bilayers do recover upon photobleaching. Upon bilayer formation, the solution contained within the dish was exchanged 5 times with 2 mL aliquots of the buffer solution. Following rinsing, I was adjusted to 0.025 M.

REFERENCES

(1) Richards, S. M.; Strandberg, K. L.; Gunn, J. S. *Salmonella*-Regulated Lipopolysaccharide Modifications. *Sub-cellular Biochem.* **2010**, *53*, 101–122.
(2) Raetz, C. R. H.; Whitfield, C. Lipopolysaccharide Endotoxins. *Annu. Rev. Biochem.* **2002**, *71*, 635–700.
(3) Strain, S. M.; Armitage, I. M. Selective Detection of 3-Deoxymannooctulosonic Acid in Intact Lipopolysaccharides by Spin-Echo 13C NMR. *J. Biol. Chem.* **1985**, *260*, 12974–12977.
(4) Kirschner, K. N.; Lins, R. D.; Maass, A.; Soares, T. A. A Glycam-Based Force Field for Simulations of Lipopolysaccharide Membranes: Parametrization and Validation. *J. Chem. Theory Comput.* **2012**, *8*, 4719–4731.
(5) Rittig, M. G. Smooth and Rough Lipopolysaccharide Phenotypes of *Brucella* Induce Different Intracellular Trafficking and Cytokine/chemokine Release in Human Monocytes. *J. Leukoc. Biol.* **2003**, *74*, 1045–1055.
(6) Karkhanis, Y. D.; Zeltner, J. Y.; Jackson, J. J.; Carlo, D. J. A New and Improved Microassay to Determine 2-Keto-3-Deoxyoctonate in Lipopolysaccharide of Gram-Negative Bacteria. *Anal. Biochem.* **1978**, *85*, 595–601.
(7) Sauerbrey, G. Verwendung von Schwingquarzen Zur Wägung Dünner Schichten Und Zur Mikrowägung. *Z. Phys.* **1959**, *155*, 206–222.
(8) Reviakine, I.; Johannsmann, D.; Richter, R. P. Hearing What You Cannot See and Visualizing What You Hear: Interpreting Quartz Crystal Microbalance Data from Solvated Interfaces. *Anal. Chem.* **2011**, *83*, 8838–8848.
(9) Leive, L. Release of Lipopolysaccharide by EDTA Treatment of *E. coli*. *Biochem. Biophys. Res. Commun.* **1965**, *21*, 290–296.
(10) Chng, S.-S.; Ruiz, N.; Chimalakonda, G.; Silhavy, T. J.; Kahne, D. Characterization of the Two-Protein Complex in *Escherichia coli* Responsible for Lipopolysaccharide Assembly at the Outer Membrane. *Proc. Natl. Acad. Sci. U.S.A.* **2010**, *107*, 5363–5368.
(11) Galanos, C.; Luderitz, O.; Westphal, O. A New Method for the Extraction of R Lipopolysaccharides. *Eur. J. Biochem.* **1969**, *9*, 245–249.
(12) Kaufmann, S.; Ilg, K.; Mashaghi, A.; Textor, M.; Priem, B.; Aebi, M.; Reimhult, E. Supported Lipopolysaccharide Bilayers. *Langmuir* **2012**, *28*, 12199–12208.
(13) Rodahl, M.; Höök, F.; Krozer, A.; Brzezinski, P.; Kasemo, B. Quartz Crystal Microbalance Setup for Frequency and Q-Factor Measurements in Gaseous and Liquid Environments. *Rev. Sci. Instrum.* **1995**, *66*, 3924.
(14) Jacobson, K. H.; Kuech, T. R.; Pedersen, J. A. Attachment of Pathogenic Prion Protein to Model Oxide Surfaces. *Environ. Sci. Technol.* **2013**, *47*, 6925–6934.
(15) Voinova, M. V.; Rodahl, M.; Jonson, M.; Kasemo, B. Viscoelastic Acoustic Response of Layered Polymer Films at Fluid-Solid Interfaces: Continuum Mechanics Approach. *Phys. Scr.* **1999**, *59*, 391–396.
(16) Cho, N.-J.; Frank, C. W.; Kasemo, B.; Höök, F. Quartz Crystal Microbalance with Dissipation Monitoring of Supported Lipid Bilayers on Various Substrates. *Nat. Protoc.* **2010**, *5*, 1096–1106.
(17) Stumm, W.; Morgan, J. *Aquatic Chemistry: Chemical Equilibria and Rates in Natural Waters*; Wiley-Interscience, **1995**.
(18) Malin, J. N.; Hayes, P. L.; Geiger, F. M. Interactions of Ca, Zn, and Cd Ions at Buried Solid/Water Interfaces Studied by Second Harmonic Generation. *J. Phys. Chem. C* **2009**, *113*, 2041–2052.
(19) Hayes, P. L.; Chen, E. H.; Achtyl, J. L.; Geiger, F. M. An Optical Voltmeter for Studying Cetyltrimethylammonium Interacting with Fused Silica/Aqueous Interfaces at High Ionic Strength. *J. Phys. Chem.* **2009**, *113*, 4269–4280.
(20) Hayes, P. L.; Gibbs-Davis, J. M.; Musorrafiti, M. J.; Mifflin, A. L.; Scheidt, K. A.; Geiger, F. M. Environmental Biogeochemistry Studied by Second-Harmonic Generation: A Look at the Agricultural

Antibiotic Oxytetracycline. *J. Phys. Chem. C* **2007**, *111*, 8796–8804.
(21) Konek, C. T.; Illg, K. D.; Al-Abadleh, H. A.; Voges, A. B.; Yin, G.; Musorrafiti, M. J.; Schmidt, C. M.; Geiger, F. M. Nonlinear Optical Studies of the Agricultural Antibiotic Morantel Interacting with Silica/Water Interfaces. *J. Am. Chem. Soc.* **2005**, *127*, 15771–15777.